energies

MDPI

Article

Numerical Study of Thermal and Resistance Characteristics in the Vortex-Enhanced Tube

Yiang Li [1,2,3], Wenzhi Cui [1,2,*], Xuefeng Jiang [1,2,3], Longjian Li [1,2] and Juanfang Liu [1,2]

[1] School of Energy and Power Engineering, Chongqing University, Chongqing 400030, China; liyiang@sinochem.com (Y.L.); jiangxuefeng01@sinochem.com (X.J.); longjian@cqu.edu.cn (L.L.); juanfang@cqu.edu.cn (J.L.)
[2] Key Laboratory of Low-Grade Energy Utilization Technology and Systems, Chongqing University, Ministry of Education of PRC, Chongqing 400030, China
[3] Sinochem Energy Saving Technology (Beijing) Co., Ltd., Chongqing 400030, China
* Correspondence: wzcui@cqu.edu.cn

Abstract: Heat transfer enhancement is always pursued in the industry to achieve high-performance and low-energy-consumption heat exchange devices and systems. For decades, various types of heat transfer-enhancing tubes with differing geometries and wall configurations have been developed. In this paper, the heat transfer and pressure drop characteristics of air inside an innovative heat transfer tube with regular wall dimples, namely a vortex-enhanced tube, which has a great application prospect in the gas–gas heat exchanger, are numerically studied with an experimentally validated model. The effects of the depth, axial pitch, and radial rotation angle of the dimple in the tube wall on the convective heat transfer coefficient and friction drag coefficient are comprehensively analyzed. Based on the Performance Evaluation Criteria (PEC) of the tubes, the optimal parameters of the vortex-enhanced tube are obtained. When Re ranges from 10,000 to 40,000, the comprehensive evaluation factor of the vortex-enhanced tube is 1.29 times higher than the smooth tube. Dimple pacing, dimple depth, and dimple helical angle of the optimal tube type are 8 mm, 6 mm, and 83°, respectively.

Keywords: the vortex-enhanced tube; enhanced heat transfer; numerical simulation



Academic Editor: Andrea Frazzica

Received: 29 November 2024
Revised: 18 December 2024
Accepted: 19 December 2024
Published: 24 December 2024

Citation: Li, Y.; Cui, W.; Jiang, X.; Li, L.; Liu, J. Numerical Study of Thermal and Resistance Characteristics in the Vortex-Enhanced Tube. *Energies* **2025**, *18*, 13. https://doi.org/10.3390/en18010013

Copyright: © 2024 by the authors. Licensee MDPI, Basel, Switzerland. This article is an open access article distributed under the terms and conditions of the Creative Commons Attribution (CC BY) license (https://creativecommons.org/licenses/by/4.0/).

1. Introduction

Heat exchangers are widely used in power plants, petrochemicals, and food industries [1]. Tube shell-type heat exchangers are the most frequently utilized due to their straightforward structure and capacity to withstand high-pressure applications. To enhance the efficiency of heat exchange and conserve energy resources, the development of a high-performance heat exchanger device is imperative. Many high-performance heat transfer components can be realized by studying enhanced heat transfer technology, which currently, in practice, includes active and passive methods [2].

The active enhanced heat transfer technology needs to apply external force, which increases the complexity of the heat transfer process and adds more instability to the heat transfer process. The passive enhanced heat transfer technology, which is simple, energy-saving, and high safety, is widely used in industry. The passive enhanced heat transfer technology mainly includes processing rough surfaces, changing tube shape, and inserting turbulence elements in the heat transfer channels [3–6]. Among all kinds of enhanced tube structures used in convective heat transfer, the spiral structure has the advantages of saving equipment space, low production cost, and superior heat transfer performance [7,8]. The

principle behind the heat transfer enhancement of the spiral structure lies in the helical flow and secondary flow induced by the twisted curved tube wall, which changes direction, and the radial and tangential velocities that generate intense flow mixing, thereby destroying the flow boundary, so as to achieve the purpose of disrupting the flow state. The application of spiral structures, such as a twisted oval tube and a twisted tri-lobed tube, etc., [9,10] as shown in Figure 1a,b, achieve heat transfer enhancement by applying a deformation to the tube wall to change the shape of the flow section, such as an alternating cross-section flattened tube, an alternating elliptical axis tube, and dimpled tubes [11–13], as can be seen in Figure 1c,e.

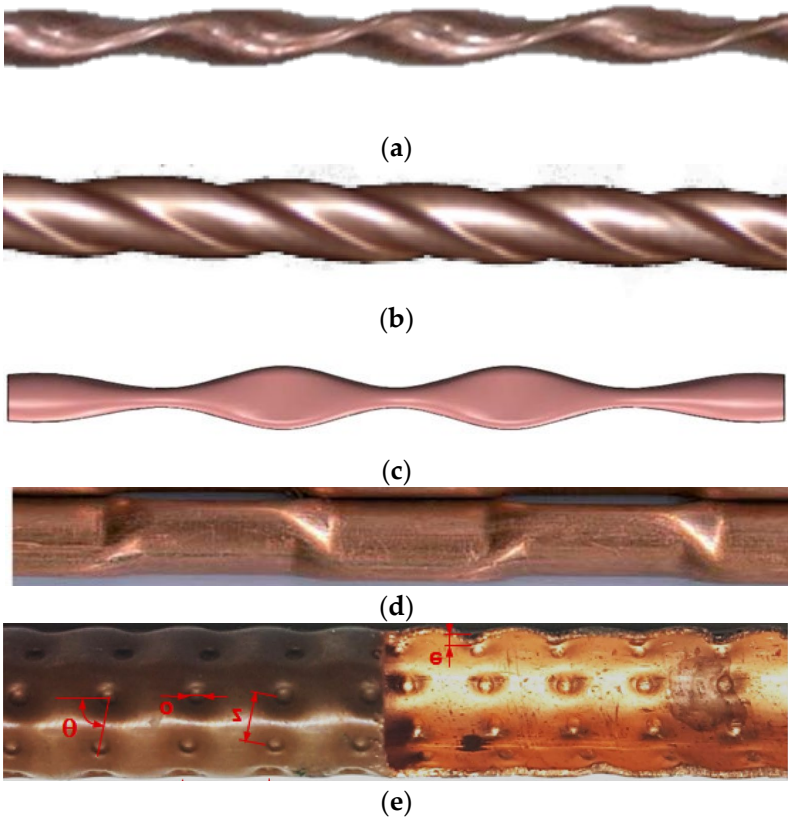


Figure 1. Geometry of different tube surfaces: (**a**) twisted oval tube, (**b**) twisted tri-lobed tube, (**c**) alternating cross-section flattened tube, (**d**) alternating elliptical axis tube, and (**e**) dimpled tubes.

The dimple tube has a special surface, which makes the flow medium produce a vortex in the process of flow, to enhance the heat transfer of the heat exchange tube [13,14]. The pits arranged on the surface by the characteristics of golf balls have a relatively low pressure drop [15–17]. The dimple tube not only enhances heat transfer performance but also minimizes resistance loss, resulting in excellent comprehensive performance.

The vortex-enhanced tube represents a newly optimized heat exchange tube, built upon the foundation of the dimple tube, featuring prominent convex and concave structures. The dimples are spirally distributed across the tube's surface, inheriting the drag-reduction characteristics of the dimple tube. Vortex-enhanced tubes have been used in industrial practice [18,19]. It has been proven that vortex-enhanced tubes can significantly increase heat transfer rates, diminish pressure drops, reduce fouling, lower processing costs, and operate without the need for additional components. In this paper, a computation model of the vortex-enhanced tube was established based on structural mechanics, and the numerical simulation was performed for different structure parameters. The findings indicated that the heat transfer rate of enhanced tubes surpassed that of smooth tubes, especially, the more excellent heat transfer enhanced performance at the low Reynolds number which was

found [20,21]. But in industrial applications, the design parameters of the heat exchanger still rely on the accumulation of experience; the structure selection of heat exchanger tubes still needs to be supported by data, such as that related to the depth of the dimple structures, pacing between the adjacent-staggered dimple structures, the intersection angle of the dimple structure, etc.

In this paper, on the basis of previous research, we optimized the tube structure by integrating the dimple structure and spiral structure, hoping to obtain a more enhanced heat transfer effect. The physical geometry model of the vortex-enhanced tube was developed through simulating the industrial production process using explicit dynamics, and numerical methods were employed to solve the turbulent flow and heat transfer within it. The objective of the study is to identify optimal design parameters that enhance the heat transfer rate while maintaining an acceptable friction factor. An optimal design is identified by comparing the comprehensive performance rate of each design, which provides a reference for the tube type selection in industrial design.

2. Numerical Model and Methods

2.1. Physical Model

Three structural parameter changes in the geometric model of the vortex-enhanced tube are shown in Figure 2. These parameters include spacing in the axial direction between the adjacent dimple structures, the depth of the dimple structure, and the rotation helix angle in the radial direction between the two adjacent dimples. The structural parameters calculated in the numerical simulation are shown in Figure 2a and Table 1.

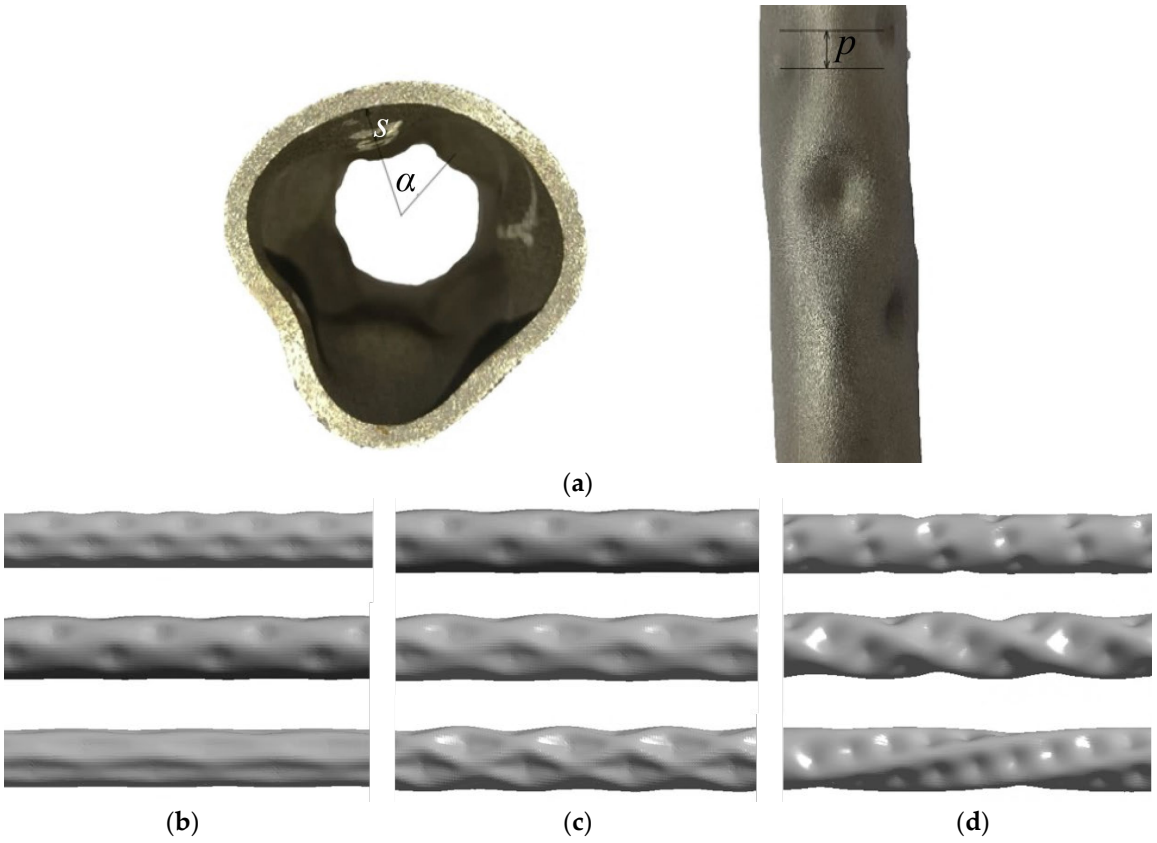


Figure 2. Schematic diagram of the structural parameter (**a**) and the vortex-enhanced tubes with the different spacing (**b**), depth (**c**), and helix angle (**d**).

Table 1. Structure parameters of the tubes.

Spacing, *p*/mm	Depth, *s*/mm	Helix Angle, *α*/°
8	3	63
11	4.5	83
14	6	103
17	7.5	133

The vortex-enhanced tube has a complex deformation of the tube wall under the action of external force. The geometric model is simulated by the explicit dynamic in ANASYS program software (version number: ANSYS 18.2) according to the actual industrial production process. It is mainly controlled by the mechanical equation, so the boundary conditions need to be set. The boundary conditions mainly involved in the model include the stress boundary conditions and the displacement boundary conditions. In this paper, the size of the tube tested in the simulation experiment is 40 mm in diameter, 1.5 mm in thickness, and 2600 mm in length. The tubular model is obtained by selecting the materials of the tube, controlling the pressing position and displacement parameters of the rigid body, and fixing the boundary conditions. A reverse flow heat transfer system is formed by adding the fluid zone inside and outside the tube model, as shown in Figure 3.

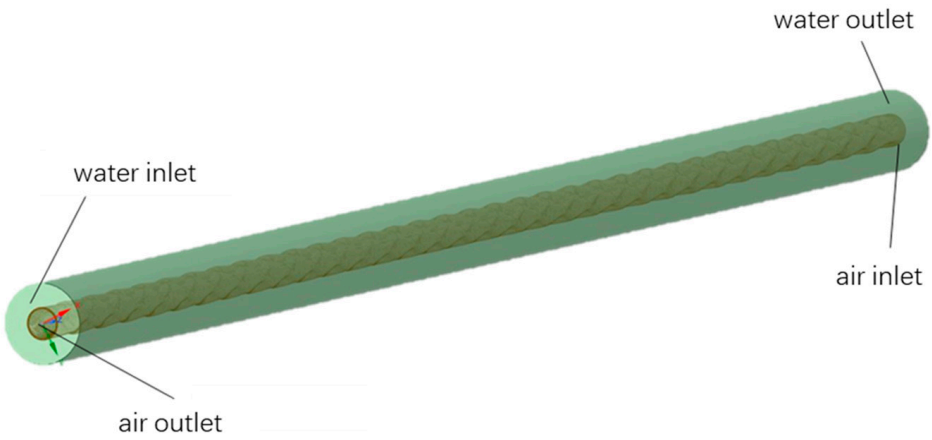


Figure 3. Physical model of the vortex-enhanced tube heat exchange system.

2.2. Governing Equations and Boundary Conditions

According to the actual processing structure of the vortex-enhanced tube, the following assumptions are made to ensure that the flow and heat transfer characteristics of the system are not adversely affected: (1) the working fluid is considered incompressible and has constant properties; (2) fluid physical parameters remain unchanged; (3) the effects of the gravitational field and heat radiation are neglected.

The Reynolds-averaged Navier–Stokes (RANS) equations for the turbulent convective heat transfer into the heat exchanger at the steady state are expressed with tensor form as follows:

Continuity equation:

$$\frac{\partial\left(\rho\overline{u_j}\right)}{\partial x_j} = 0 \tag{1}$$

Momentum equation:

$$\frac{\partial\left(\rho\overline{u_i}\,\overline{u_j}\right)}{\partial x_j} = -\frac{\partial\overline{p}}{\partial x_i} + \frac{\partial}{\partial x_j}\left[\mu\left(\frac{\partial\overline{u_j}}{\partial x_i} + \frac{\partial\overline{u_i}}{\partial x_j}\right) - \frac{2}{3}\delta_{ij}\frac{\partial u_l}{\partial u_l}\right] + \frac{\partial}{\partial x_j}\left(-\rho\overline{u_i'u_j'}\right) \tag{2}$$

Energy equation:

$$\frac{\partial(\overline{u_i}\,\overline{T})}{\partial x_i} = \frac{\partial}{\partial x_i}\left[\left(\lambda + \frac{\mu_t}{Pr_t}\frac{\partial \overline{T}}{\partial x_i}\right)\right] \tag{3}$$

where λ is thermal conductivity, W/(m·K), μ is dynamic viscosity, and Pa·s, ρ is the density. $\overline{u_i}$ (I = 1,2,3) is the time average velocity in Cartesian coordinate, respectively. The additional term $-\rho\overline{u_i'u_j'}$ in Equation (2) is called the Reynolds stress, which is resolved with the realizable k-ε model [22,23]. μ_t and Pr_t in Equation (3) are the turbulent (or eddy) viscosity and the turbulent Prandtl number, respectively.

The realizable k-ε model is chosen to simulate turbulent flow. The enhanced wall function method is used for the near-wall treatment. Liquid water is assigned as the fluid outside the tube, while air is designated as the fluid inside the tube, and the following boundary conditions are established. Given the pressure outlet and velocity inlet, the air inlet temperature is 298.15 K, and the inlet temperature of liquid water is 363.15 K. The velocity inlet of air is set as 5–15 m/s, which is the air velocity of the tube inside, common in industry, the mass flow rate in the corresponding working condition is about 15–65 m^3/h, and the velocity inlet of water is set as 1 m/s. Pressure–velocity coupling is chosen for the SIMPLE scheme, spatial discretization is established as second-order upwind for momentum, and turbulent kinetic energy is selected. The convergence absolute criteria condition was set to less than 10×10^{-6}.

2.3. Parameter Definitions

The flow and heat transfer characteristics of the fluid inside the vortex-enhanced tube were evaluated using the following dimensionless parameters.

Reynolds number

$$Re = \frac{\rho u_m D}{\mu} \tag{4}$$

Nusselt number

$$Nu = \frac{hD}{\lambda} \tag{5}$$

Darcy friction factor

$$f = \frac{\Delta p D}{\frac{1}{2}\rho u_m^2 L} \tag{6}$$

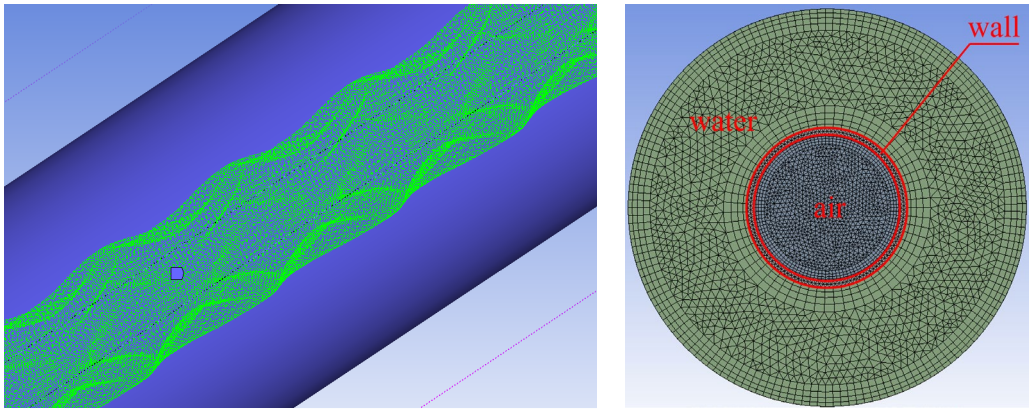
Here, h is the heat transfer coefficient, W/(m^2·K), D is the vortex-enhanced tube equivalent diameter, mm. The thermal performance factor was utilized to assess the overall performance of the tube [24]. The subscript "0" indicates the value obtained from the smooth tube.

$$\eta = (Nu/Nu_0)/(f/f_0)^{1/3} \tag{7}$$

2.4. Grid Details and Grid Mesh Independent Test

This model adopts a Mesh module of ANASYS program for discretization. Since the geometric model was obtained through explicit dynamics calculation, it will produce drastic geometric structure changes on the surface of the dimple. Unstructured grids were adopted for discretization of the geometric model and mesh refinement. A refined boundary layer grid was generated near the basin wall to satisfy the application requirements of the wall function method. The size of the tube inside the grid was set as 1 mm, the size of the vortex-enhanced tube grid was set as 1 mm, and the size of the tube outside the grid was set as 2 mm. The surface mesh of the vortex-enhanced tube is shown in Figure 4a. Set the boundary layer: the inner tube coupled with tube wall faces inward expansion, the outer tube coupled with the wall faces outward expansion, and the outer faces inward expansion.

Set the transition ratio of expansion parameters as 0.9, the maximum layers as 4, and the growth rate as 1.2. The generated mesh is shown in Figure 4b.



(**a**) (**b**)

Figure 4. (**a**) Surface mesh of the vortex-enhanced tube, (**b**) mesh system of the cross-section.

Through the grid mesh independent test, the reasonable mesh design is selected. Table 2 shows the calculation parameters of mesh independence verification. When the number of grids is greater than 9.21×10^6, the relative error of heat transfer coefficient h and resistance coefficient f is less than 4%, so this grid setting is selected for subsequent calculation.

Table 2. The calculation parameters of mesh independence verification.

Grid	*Nu*	*f*
35,569,065	43.508	0.110772432
21,585,632	43.092	0.110762432
9,211,630	42.561	0.110743776
5,322,560	28.673	0.110532707

2.5. Validation

To validate the numerical method used in this study, the thermal-hydraulic performance of a vortex-enhanced tube was calculated and compared against experimental data under identical boundaries and geometrical conditions. The experimental platform's primary components of the system include a fan, a thermostat-controlled hot water tank, a circulating pump, and an annular tube heat exchanger. The heat exchanger is composed of an annular tube and the experimental tube. Hot water at 95 °C flows through the shell side, while cold air passes through the tube side. The air inside the experimental tube is warmed by the hot water circulating outside the tube. The range of *Re* is 10,000 to 40,000, the *Nu* comparison results as shown in Figure 5, the calculated values of *Nu* are slightly higher than the experimental results. However, the variation trends with Re remain consistent, with a maximum relative error of 3.0%. The comparison results are shown in Figure 6. The variation trends with *Re* are consistent, and the maximum relative error for f is 6.3%. This comparison demonstrates that the numerical results align well with the experimental data.

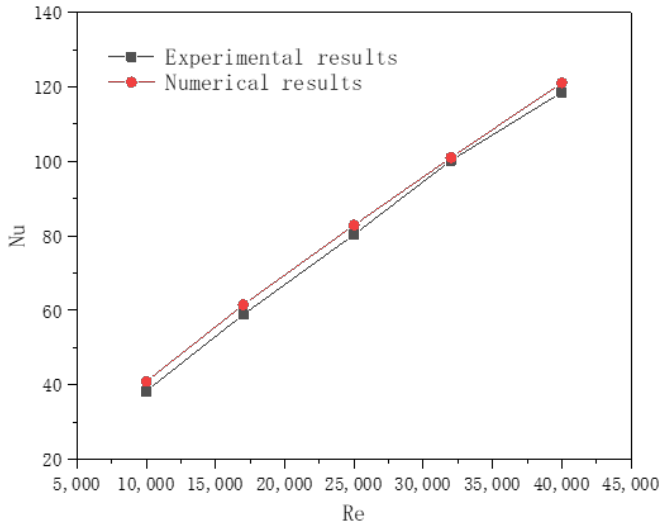


Figure 5. Comparison of the *Nu* of numerical and experimental results.

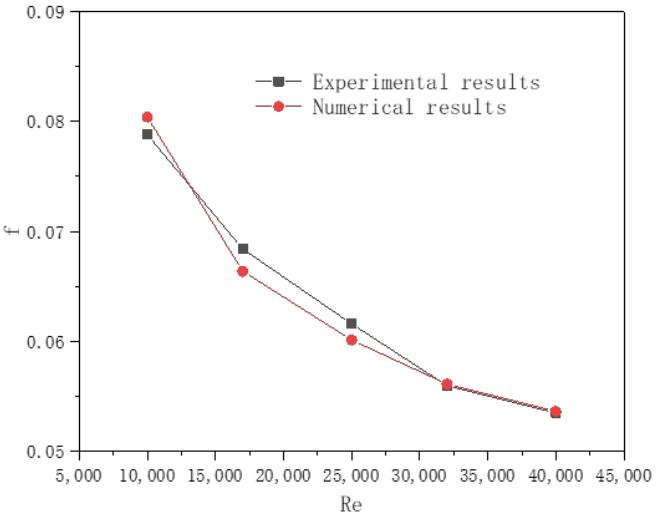


Figure 6. Comparison of the f of numerical and experimental results.

3. Results and Discussion

3.1. Influence of the Dimple Spacing

Axial dimple spacing is the distance between two adjacent vortices along the tube axis, The smaller the dimple spacing, the more compact the axial dimple arrangement. When the dimple spacing is changed, the other two structural parameters remain unchanged: the dimple depth is 6 mm, and the dimple helical angle is 103°.

Figure 7 shows that *Nu* increases with *Re* (10,000–40,000) and is consistently higher for vortex-enhanced tubes compared to smooth tubes, highlighting their superior heat transfer. The 8 mm spacing achieves the highest *Nu*, 35.11% higher than the smooth tube, while the 17 mm spacing shows the smallest improvement (28.45%). Smaller spacing does not always guarantee better performance, as the 14 mm spacing outperforms the 11 mm spacing. The magnitude and direction of the fluid velocity continuously fluctuate, with the velocity increasing in radial flow. As a result, the flow boundary layer experiences constant disruption, maintaining a thin and discontinuous state. This dynamic interaction promotes strong mixing between the mainstream fluid and the near-wall fluid. The flow field alterations caused by the dimple structure disturb the boundary layer, thereby enhancing heat transfer.

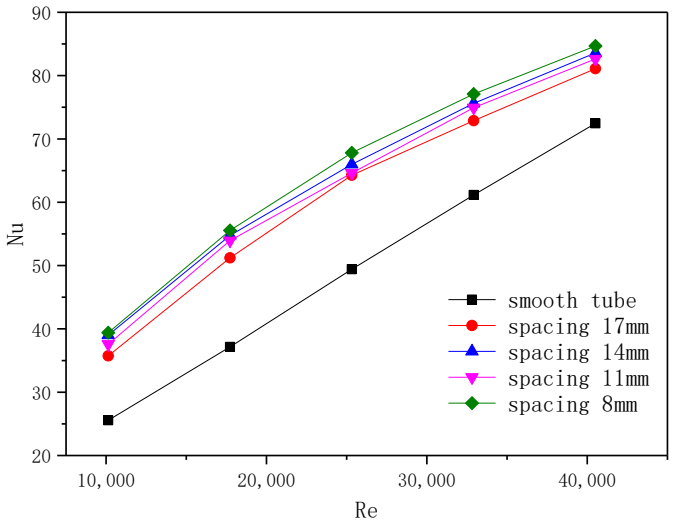


Figure 7. Variation in *Nu* with *Re* for the vortex-enhanced tubes with varying dimple spacing.

Figure 8 shows the influence of varying dimple spacing on Nu/Nu_0, and Nu/Nu_0 shows a decreasing trend with *Re*, indicating that when *Re* is lower, the variation in dimple spacing has a more obvious influence on heat transfer performance. The effect of dimple spacing on Nu/Nu_0 is the same as that on *Nu*.

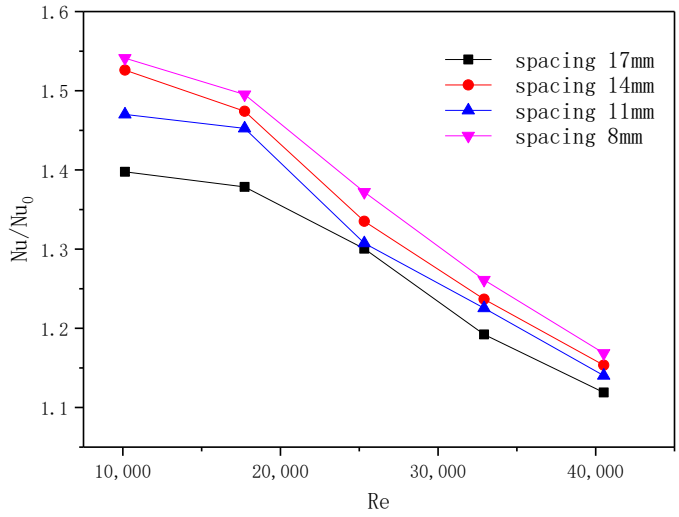


Figure 8. Variation in Nu/Nu_0 with *Re* for the vortex-shaped tubes with varying dimple spacing.

Figure 9 shows that the friction factor decreases with increasing Re. The smooth tube's friction factor ranges from 0.019 to 0.030, while the vortex-enhanced tube ranges from 0.022 to 0.053 due to increased surface roughness. The difference in friction factors is minimal, varying between 0.36% and 4.94%.

As shown in Figure 10, f/f_0 decreases with the increase in Re, indicating that the change in dimple spacing has a more obvious influence on the resistance when *Re* is in a low range. The change in f/f_0 is negligible between different spacing. It shows that the structure parameter of dimple spacing has little influence on the resistance.

Figure 11 shows that the efficiency factor (η) varies with dimple spacing and *Re*. The 8 mm dimple spacing tube achieves the highest η (1.12–1.27), decreasing slowly with *Re* until 17,000, after which it declines significantly. For the 11 mm and 17 mm tubes, η initially increases, peaking at higher *Re* (17,000 and 25,000, respectively), before decreasing. The 14 mm tube shows a trend similar to the 8 mm tube but with slightly lower η. Across all

cases, η first rises and then declines, with lower η tubes requiring higher *Re* to reach their peak efficiency.

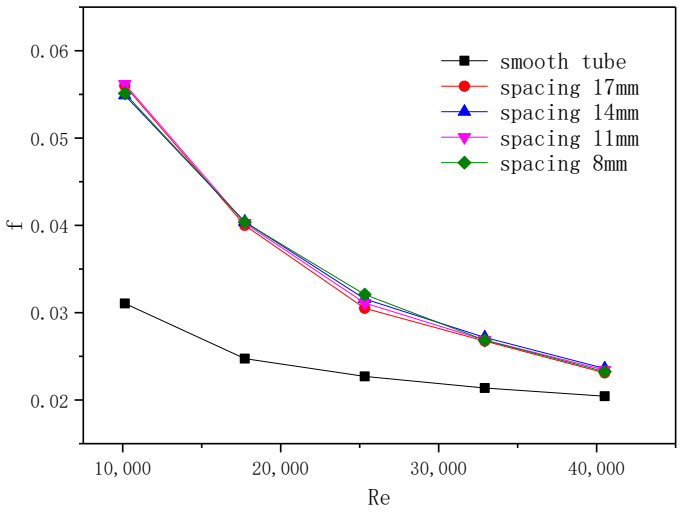


Figure 9. Variation in f with *Re* for the vortex-enhanced tubes with varying dimple spacing.

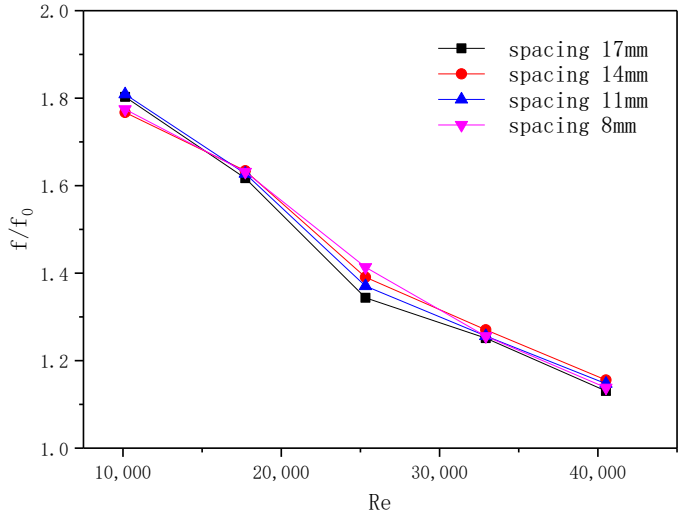


Figure 10. Variation in f/f_0 with *Re* for the vortex-enhanced tubes with varying dimple spacing.

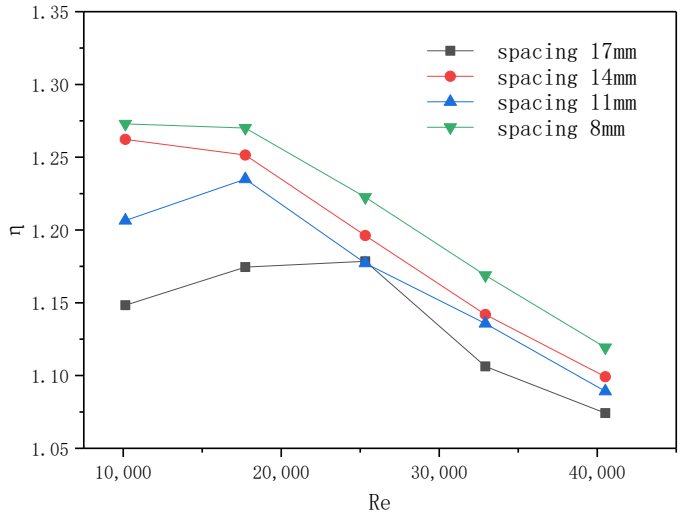


Figure 11. Variation in η with *Re* for the vortex-enhanced tubes with varying dimple spacing.

The η values of the vortex-enhanced tube are greater than 1, indicating that it effectively enhances heat transfer. As the fluid flows through the dimple structure on the tube surface, its velocity direction changes radially, which increases turbulence intensity. As the dimple spacing increases, the resistance of the vortex-enhanced tube decreases, along with a reduction in *Nu*. This occurs because, as the fluid passes through the dimple, the change in cross-sectional area generates local resistance at the dimple. When dimple spacing increases, fewer dimple structures are present per unit length, leading to reduced flow resistance. Simultaneously, as the number of vortices decreases, the fluid experiences fewer disturbances, weakening the heat transfer enhancement effect.

3.2. Influence of the Dimple Depth

When the dimple depth is changed, the other two structural parameters remain unchanged; the dimple spacing is 11 mm and the dimple helical angle is 103°.

Figure 12 shows that as dimple depth increases from 3 mm to 7.5 mm, the *Nu* of the vortex-enhanced tube increases, indicating stronger heat transfer performance. The *Nu* of the vortex-enhanced tube is consistently higher than the smooth tube, especially at high *Re*. The deepest dimple (7.5 mm) shows the most significant improvement, with a *Nu* increase of 43.3% to 48.8%, compared to the smooth tube. Smaller dimple depths (3 mm, 4.5 mm, and 6 mm) show increases ranging from 13.0% to 40.5%, highlighting the positive effect of deeper dimple structures on heat transfer performance.

Figure 13 shows that Nu/Nu_0 increases slightly before *Re* exceeds 17,000 and then remains nearly constant, with changes ranging from 0.4% to 2.1%. Deeper dimple depths result in higher Nu/Nu_0 values.

Figure 14 shows that the friction factor (f) is higher at low *Re* and decreases gradually with increasing *Re*. The friction factor of the vortex-enhanced tube is greater than that of the smooth tube, with deeper dimple depths resulting in higher friction factors. For a dimple depth of 7.5 mm, f ranges from 0.078 to 0.111, 73.3% to 75.1% higher than the smooth tube. For 6 mm, f ranges from 0.049 to 0.071, 58.2% to 60.3% higher; for 4.5 mm, f ranges from 0.033 to 0.048, 38.4% to 41.7% higher; and for 3 mm, f ranges from 0.024 to 0.033, 10.3% to 18.4% higher.

As shown in Figure 15, f/f_0 at each dimple depth changes gently with *Re*. The deeper dimple depth tube has a higher f/f_0 with the smooth tube. The f of the 7.5 mm dimple depth tube is significantly higher than that of other tubes.

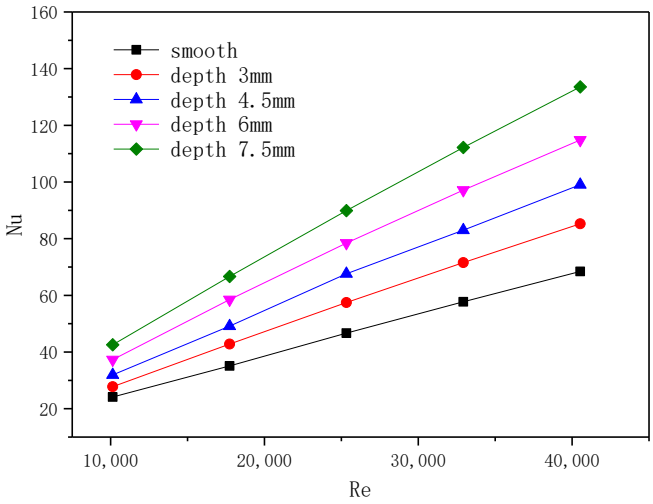


Figure 12. Variation in *Nu* with *Re* for the vortex-enhanced tubes with varying dimple depth.

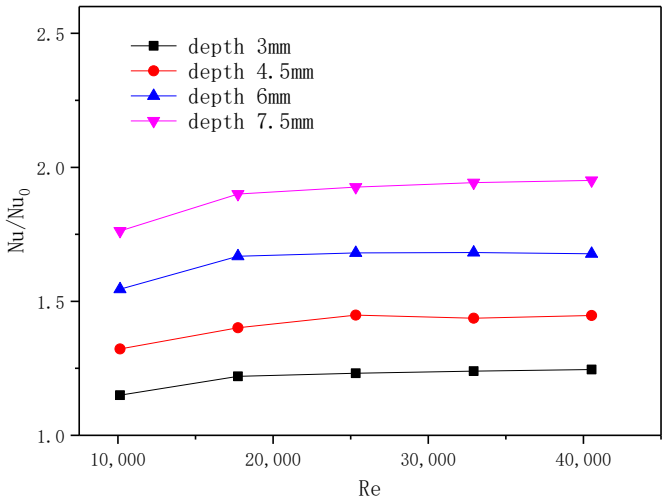


Figure 13. Variation in Nu/Nu_0 with Re for the vortex-enhanced tubes with varying dimple depth.

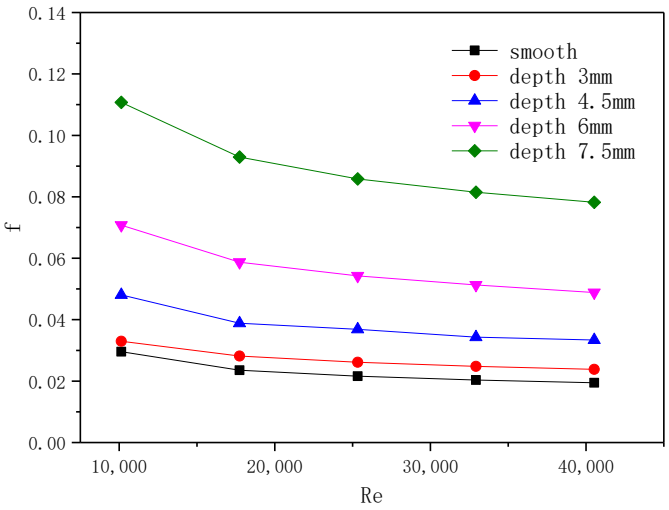


Figure 14. Variation in f with Re for the vortex-enhanced tubes with varying dimple depth.

Figure 16 shows that η is low at low Re and levels off after Re reaches 17,000. The highest η occurs with a dimple depth of 6 mm, with a change range of only 0.51% after Re 17,000 and an average value of 1.23. The η of 7.5 mm and 4.5 mm dimple depth tubes after Re 17,000 are 1.22 and 1.20, respectively. The 3 mm dimple depth tube has the lowest η, with an average value of 1.16 after Re 17,000. The dimple depth's effect on η increases significantly until reaching a critical value between 3 and 4.5 mm, after which the impact diminishes.

As the dimple depth increases, the Nu and f of the vortex-enhanced tube also increase. The vortex depth of 6 mm has the highest η. With the dimple depth increasing, the resistance continues to increase, while the heat transfer increases to a lesser extent, thus its η decreases. Therefore, when the dimple depth is 6 mm, the vortex-enhanced tube has the extreme value of η. The dimple depth has a large impact on the flow heat transfer performance; the reason is that when the dimple depth increases, the cross-sectional area of the heat exchanger tube decreases and the flow channel becomes narrower, thus increasing the resistance, and at the same time, because of the existence of the vortex, its disturbance increases, and heat transfer is enhanced.

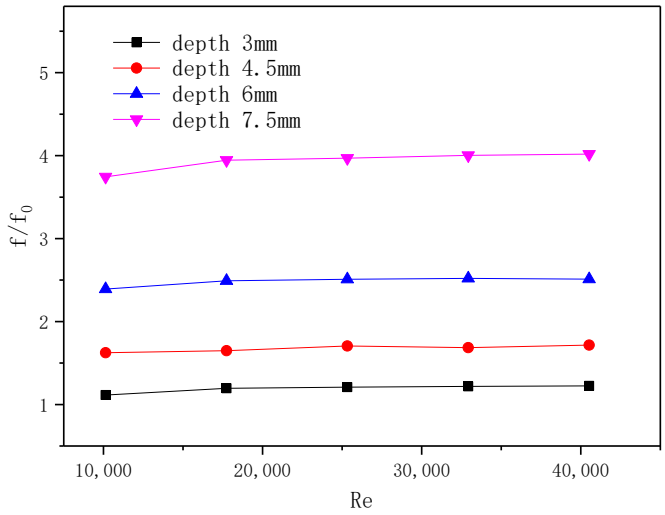


Figure 15. Variation in f/f_0 with *Re* for the vortex-enhanced tubes with varying dimple depth.

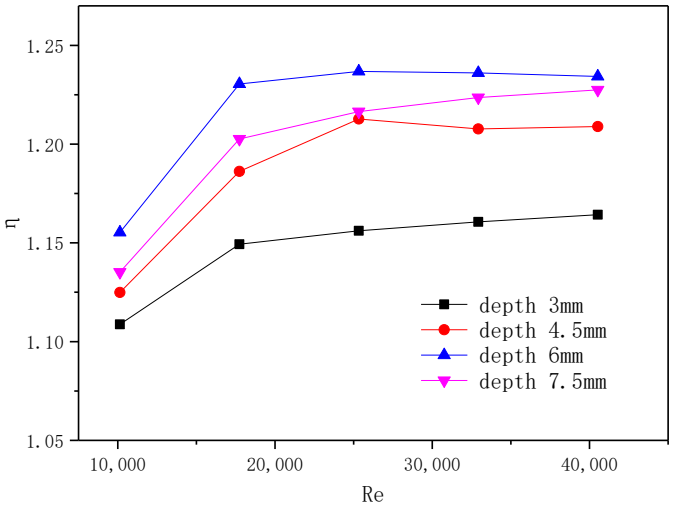


Figure 16. Variation in η with *Re* for the vortex-enhanced tubes with varying dimple depth.

3.3. Influence of the Dimple Helical Angle

The dimple helical angle has a complicated influence on the structure of the vortex-enhanced tube. The structural parameters commonly used in industrial design are selected for comparison, so as to select the optimal dimple helical angle parameters. When the dimple helical angle is changed, the other two structural parameters remain unchanged: the dimple depth is 6 mm and the dimple spacing is 11 mm.

As shown in Figure 17, *Nu* increases positively with *Re*. The *Nu* of the dimple helical angle of 63° and 83° is similar and relatively higher, and the *Nu* of the dimple helical angle of 103° and 133° is similar. The heat transfer performance of the tube is stronger at high Re. With the increase in *Re*, *Nu* of the vortex-enhanced tube was increased relative to the smooth tube. the dimple helical angle of 63°, 83°, 103°, and 133° were increased, respectively, by 41.0–43.7%, 39.6–43.7%, 36.5–40.2%, and 34.9–40.1%.

As shown in Figure 18, each dimple helical angle tube has an obvious increase trend with *Re* at low *Re* range of 10,000 to 17,000, and a gentle increase trend at high *Re*.

Figure 19 shows that the friction factor (f) is higher at low *Re* and decreases gradually with increasing *Re*. The tube with a 63° dimple helical angle has the highest f, ranging from 0.054 to 0.080, 63.21% to 63.71% higher than the smooth tube.

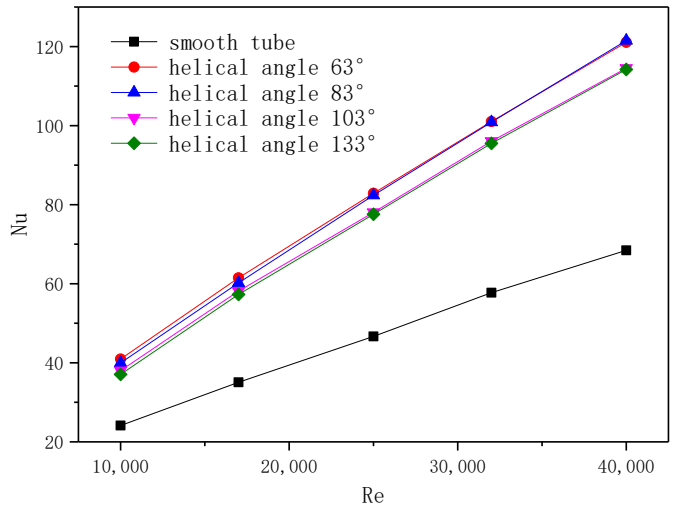


Figure 17. Variation in *Nu* with *Re* for the vortex-enhanced tubes with varying dimple helical angle.

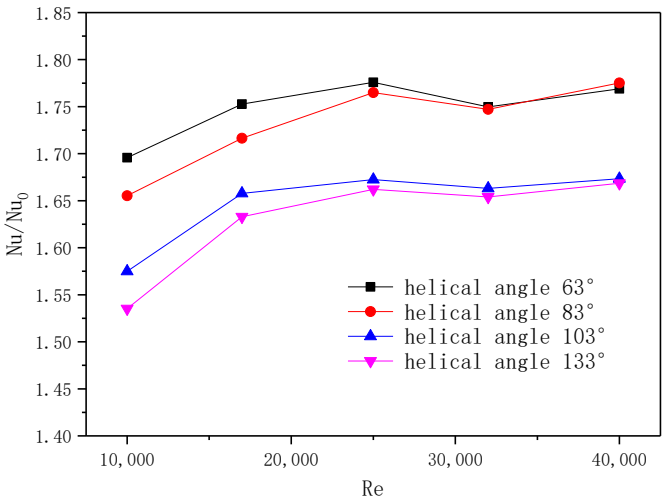


Figure 18. Variation in Nu/Nu_0 with *Re* for the vortex-enhanced tubes with varying dimple helical angle.

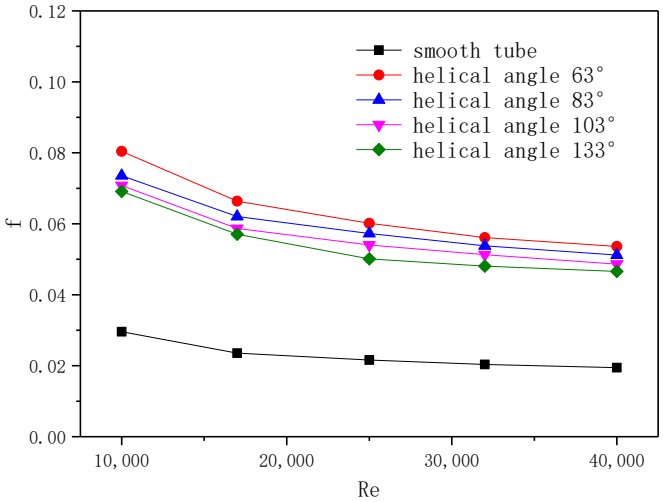


Figure 19. Variation in f with *Re* for the vortex-enhanced tubes with varying dimple helical angle.

As shown in Figure 20, f/f_0 at each dimple helical angle changes gently with *Re*. The influence of dimple helical angle on f/f_0 is consistent with the influence trend on the *Nu*

ratio. The tube with large Nu/Nu_0 has relatively large f/f_0, and the average f/f_0 of the 63–103° tube is 2.77, 2.61, 2.48, and 3.37, respectively.

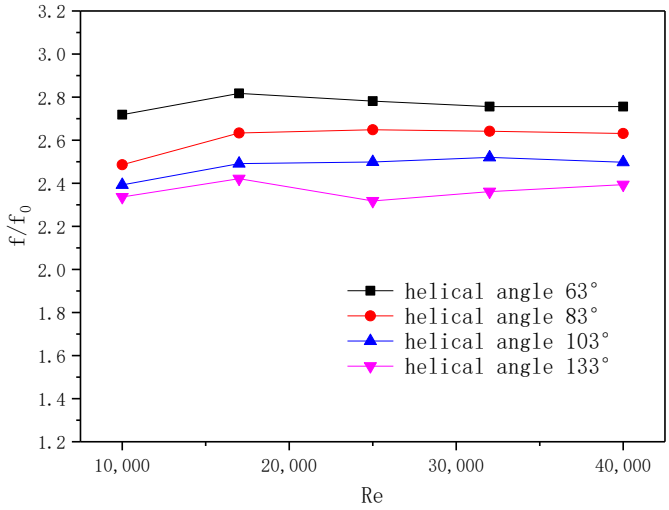


Figure 20. Variation in f/f_0 with *Re* for the vortex-enhanced tubes with varying dimple helical angle.

As can be seen from Figure 21, with the *Re* increase, η firstly increases and then flattens. The η of the tube with 83° dimple helical angle is stronger than that of other tube types, and the average η is 1.26. η of the tube with 103° and 133° dimple helical angle is low, and η are both 1.22. However, the η of the tube with a 103° dimple helical angle is higher when the *Re* is below 17,000. With the increase in *Re*, the η of the tube with a 133° dimple helical angle is higher than that of 103°.

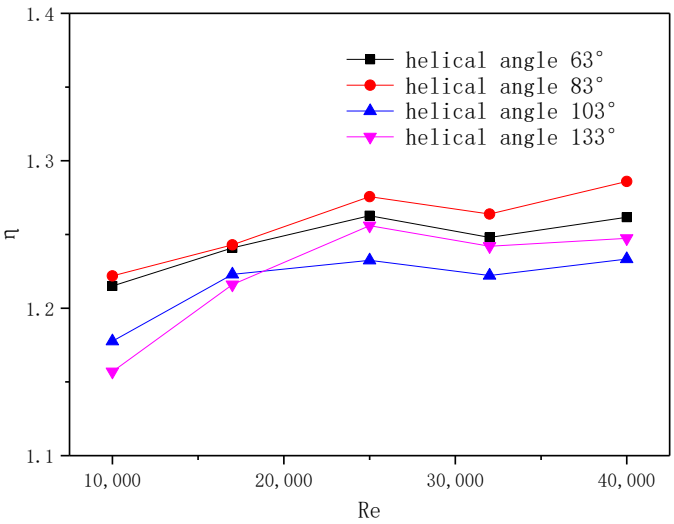


Figure 21. Variation in η with *Re* for the vortex-enhanced tubes with varying dimple helical angles.

With the decrease in the dimple helical angle, the spacing between the adjacent dimple structure is narrowed and the overall dimple distribution is dense. At this time, the spiral channel inside the tube is more compact and obvious, and the degree of the mainstream helix and the rotational secondary flow are enhanced, causing stronger perturbations to the inner tube fluid and further strengthening the effect of heat transfer. Meanwhile, the circumferential densification of the dimple structure leads to the increase in surface roughness and the decrease in cross-sectional area, which increases flow resistance in the tube. Notably, the effect of the dimple helical angle is complex. When the helical angle is a special angle, such as 30°, 45°, etc., the dimple pits are arranged in a straight line in the axial direction and the spiral structure becomes invalid, decreasing in flow field disturbance and

deteriorating heat transfer. And when the dimple helical angle is closer to the special angle, the heat transfer enhancement will also be weakened.

4. Conclusions

In this paper, the explicit dynamic module of ANSYS was adopted, and highly realistic physical models of the vortex-enhanced tube were established by simulating the real processing of the vortex-enhanced tube with the finite element method. The influence of the structural parameters and operating conditions on heat transfer characteristics and flow resistance in the vortex-enhanced tube was studied by using the control parameter method. On the basis of the previous research, the new tube type combined with the dimple structure and the spiral structure were studied. When the comprehensive evaluation factor is almost the same, the resistance is greatly reduced, which plays a favorable optimization role in industrial applications that value total resistance. Finally, the optimal tube type was determined. The main conclusions of this paper are as follows:

1. Due to the unique dimple structure, the vortex-enhanced tube yields superior heat transfer performance and a higher comprehensive evaluation factor compared to the smooth tube. In the heat exchanger design, the vortex-enhanced tube was able to replace the smooth tube in the heat exchange equipment at normal temperature and pressure, thereby reducing total resistance and enhancing heat transfer by increasing the heat transfer coefficient while minimizing the required tube length.
2. When *Re* ranges from 10,000 to 40,000, and within the tested dimple spacing range, the *Nu*, *f* and comprehensive evaluation factor of the vortex-enhanced tube was 1.12–1.54 times, 1.13–1.18 times, and 1.07–1.27 times higher than the smooth tube, respectively; within the tested dimple depth range, the *Nu*, *f*, and comprehensive evaluation factor of the vortex-enhanced tube was 1.15–1.95 times, 1.11–4.02 times, and 1.11–1.24 times higher than the smooth tube, respectively; within the tested dimple helical angle range, the *Nu*, *f*, and comprehensive evaluation factor of the vortex-enhanced tube was 1.54–1.78 times, 2.32–2.82 times, and 1.16–1.29 times higher than the smooth tube, respectively.
3. Several important structural parameters of the vortex-enhanced tube were experimented and the simulation results were compared with the experimental data. The optimal independent structure parameter was determined when the other two parameters were fixed through the comparative analysis, and the dimple spacing, dimple depth, and dimple helical angle of the optimal tube type were 8 mm, 6 mm, and 83°, respectively.

Author Contributions: Y.L.: Conceptualization, methodology, data reduction, writing and revision-original draft, review and editing, and visualization. W.C.: Conceptualization, methodology, resources, supervision, review and editing. X.J.: Experimental platform construction and data collection. L.L.: Conceptualization, methodology, supervision and review. J.L.: Methodology, review and editing. All authors have read and agreed to the published version of the manuscript.

Funding: This research received no external funding.

Data Availability Statement: Data will be made available upon reasonable request.

Conflicts of Interest: Authors Yiang Li and Xuefeng Jiang were employed by the company Sinochem Energy Saving Technology (Beijing) Co., Ltd. The remaining authors declare that the research was conducted in the absence of any commercial or financial relationships that could be construed as a potential conflict of interest.

References

1. Ji, W.T.; Jacobi, A.M.; He, Y.L.; Tao, W.Q. Summary and Evaluation on the Heat Transfer Enhancement Techniques of Gas Laminar and Turbulent Pipe Flow. *Int. J. Heat Mass Transf.* **2017**, *111*, 467–483. [CrossRef]
2. Bergles, A.E.; Manglik, R.M. Current Progress in Enhanced Heat and Mass Transfer. In Proceedings of the ASME 2012 Heat Transfer Summer Conference collocated with the ASME 2012 Fluids Engineering Division Summer Meeting and the ASME 2012 10th International Conference on Nanochannels, Microchannels, and Minichannels, Rio Grande, PR, USA, 8–12 July 2012; Volume 2, pp. 115–124. [CrossRef]
3. Yang, S.; Zhang, L.; Xu, H. Experimental Study on Convective Heat Transfer and Flow Resistance Characteristics of Water Flow in Twisted Elliptical Tubes. *Appl. Therm. Eng.* **2011**, *31*, 2981–2991. [CrossRef]
4. Chen, Z.-Y.; Cheng, M.; Liao, Q.; Ding, Y.D.; Zhang, J.N. Experimental Investigation on the Air-Side Flow and Heat Transfer Characteristics of 3-D Finned Tube Bundle. *Int. J. Heat Mass Transf.* **2019**, *131*, 506–516. [CrossRef]
5. Aroonrat, K.; Jumpholkul, C.; Leelaprachakul, R.; Dalkilic, A.S.; Mahian, O.; Wongwises, S. Heat Transfer and Single-Phase Flow in Internally Grooved Tubes. *Int. Commun. Heat Mass Transf.* **2013**, *42*, 62–68. [CrossRef]
6. Eiamsa-ard, S.; Promvonge, P. Heat Transfer Characteristics in a Tube Fitted with Helical Screw-Tape with/without Core-Rod Inserts. *Int. Commun. Heat Mass Transf.* **2007**, *34*, 176–185. [CrossRef]
7. Eiamsa-ard, S.; Promthaisong, P.; Thianpong, C.; Pimsarn, M.; Chuwattanakul, V. Influence of Three-Start Spirally Twisted Tube Combined with Triple-Channel Twisted Tape Insert on Heat Transfer Enhancement. *Chem. Eng. Process. Process Intensif.* **2016**, *102*, 117–129. [CrossRef]
8. Pidaparthi, B.; Li, P.; Missoum, S. Entropy-Based Optimization for Heat Transfer Enhancement in Tubes with Helical Fins. *J. Heat Transf.* **2022**, *144*, 12001. [CrossRef]
9. Tang, X.; Dai, X.; Zhu, D. Experimental and Numerical Investigation of Convective Heat Transfer and Fluid Flow in Twisted Spiral Tube. *Int. J. Heat Mass Transf.* **2015**, *90*, 523–541. [CrossRef]
10. Zhang, L.; Yang, S.; Xu, H. Experimental Study on Condensation Heat Transfer Characteristics of Steam on Horizontal Twisted Elliptical Tubes. *Appl. Energy* **2012**, *97*, 881–887. [CrossRef]
11. Rukruang, A.; Chimres, N.; Kaew-On, J.; Wongwises, S. Experimental and Numerical Study on Heat Transfer and Flow Characteristics in an Alternating Cross-section Flattened Tube. *Heat Transf. Res.* **2019**, *48*, 817–834. [CrossRef]
12. Meng, J.-A.; Liang, X.-G.; Chen, Z.-J.; Li, Z.-X. Experimental Study on Convective Heat Transfer in Alternating Elliptical Axis Tubes. *Exp. Therm. Fluid Sci.* **2005**, *29*, 457–465. [CrossRef]
13. Aroonrat, K.; Wongwises, S. Experimental Investigation of Condensation Heat Transfer and Pressure Drop of R-134a Flowing inside Dimpled Tubes with Different Dimpled Depths. *Int. J. Heat Mass Transf.* **2019**, *128*, 783–793. [CrossRef]
14. Wang, Y.; He, Y.-L.; Lei, Y.-G.; Zhang, J. Heat Transfer and Hydrodynamics Analysis of a Novel Dimpled Tube. *Exp. Therm. Fluid Sci.* **2010**, *34*, 1273–1281. [CrossRef]
15. García, A.; Solano, J.P.; Vicente, P.G.; Viedma, A. The Influence of Artificial Roughness Shape on Heat Transfer Enhancement: Corrugated Tubes, Dimpled Tubes and Wire Coils. *Appl. Therm. Eng.* **2012**, *35*, 196–201. [CrossRef]
16. Leontiev, A.I.; Kiselev, N.A.; Burtsev, S.A.; Strongin, M.M.; Vinogradov, Y.A. Experimental Investigation of Heat Transfer and Drag on Surfaces with Spherical Dimples. *Exp. Therm. Fluid Sci.* **2016**, *79*, 74–84. [CrossRef]
17. Huang, Z.; Yu, G.L.; Li, Z.-Y.; Tao, W.-Q. Numerical Study on Heat Transfer Enhancement in a Receiver Tube of Parabolic Trough Solar Collector with Dimples, Protrusions and Helical Fins. *Energy Procedia* **2015**, *69*, 1306–1316. [CrossRef]
18. Sinochem Environment Holdings Co. Ltd. Available online: http://www.sinochemehc.com/18403.html (accessed on 5 October 2024).
19. Peterseim, J.H.; Hellwig, U.; Endrullat, K. Parallel Flow Boiler Designs to Minimise Erosion and Corrosion from Dust Loaded Flue Gases. In Proceedings of the ASME Power Conference, American Society of Mechanical Engineers. Boston, MA, USA, 29 July–1 August 2013; p. V001T02A002. [CrossRef]
20. Liu, J.; Chen, S.; Gan, M.; Chen, Q. Heat Transfer and Flow Resistance Characteristics inside an Innovative Vortex Enhanced Tube. *Appl. Therm. Eng.* **2018**, *144*, 702–710. [CrossRef]
21. Chen, S.; Liu, J.; Chen, H.; Chen, Q. Thermal-Hydraulic Characteristics of the Fluid inside the Innovative Vortex-Shaped Tubes with the Different Geometrical Parameters. *Appl. Therm. Eng.* **2019**, *146*, 588–599. [CrossRef]
22. Negoescu, C.C.; Li, Y.; Al-Duri, B.; Ding, Y. Heat Transfer Behaviour of Supercritical Nitrogen in the Large Specific Heat Region Flowing in a Vertical Tube. *Energy* **2017**, *134*, 1096–1106. [CrossRef]

23. Al-Shamani, A.N.; Sopian, K.; Mohammed, H.A.; Mat, S.; Ruslan, M.H.; Abed, A.M. Enhancement Heat Transfer Characteristics in the Channel with Trapezoidal Rib–Groove Using Nanofluids. *Case Stud. Therm. Eng.* **2015**, *5*, 48–58. [CrossRef]
24. Gee, D.L.; Webb, R.L. Forced Convection Heat Transfer in Helically Rib-Roughened Tubes. *Int. J. Heat Mass Transf.* **1980**, *23*, 1127–1136. [CrossRef]

Disclaimer/Publisher's Note: The statements, opinions and data contained in all publications are solely those of the individual author(s) and contributor(s) and not of MDPI and/or the editor(s). MDPI and/or the editor(s) disclaim responsibility for any injury to people or property resulting from any ideas, methods, instructions or products referred to in the content.